High-spin structure of 102Ru

D. Sohler, J. Timar, G. Rainovski, P. Joshi, K. Starosta, D.B. Fossan, J.
Molnar, R. Wadsworth, A. Algora, P. Bednarczyk, et al.

HAL Id: in2p3-00024161
https://hal.in2p3.fr/in2p3-00024161

High-spin structure of ^{102}Ru

D. Sohler[1], J. Timár[1], G. Rainovski[2,3,*], P. Joshi[4], K. Starosta[5,2], D. B. Fossan[2,†], J. Molnár[1],
R. Wadsworth[4], A. Algora[1,6], P. Bednarczyk[7,8], D. Curien[7], Zs. Dombrádi[1], G. Duchene[7],
A. Gizon[9], J. Gizon[9], D. G. Jenkins[4], T. Koike[2,‡], A. Krasznahorkay[1], E. S. Paul[3],
P. M. Raddon[4], J. N. Scheurer[10], A. J. Simons[4], C. Vaman[2], A. R. Wilkinson[4], L. Zolnai[1]

[1]*Institute of Nuclear Research, H-4001 Debrecen, Pf. 51, Hungary,*
[2]*Department of Physics and Astronomy, SUNY, Stony Brook, New York, 11794-3800, USA,*
[3]*Oliver Lodge Laboratory, Department of Physics,*
University of Liverpool, Liverpool L69 7ZE, UK,
[4]*Department of Physics, University of York, York, YO10 5DD, UK,*
[5]*NSCL, Cyclotron Laboratory, Michigan State University, East Lansing, MI 48824-1321, USA,*
[6]*Instituto de Fisica Corpuscular, 46071 Valencia, Spain,*
[7]*IReS, 23 rue du Loess, Strasbourg, 67037, France,*
[8]*GSI, Darmstadt, Germany,*
[9]*LPSC, IN2P3-CNRS/UJF, F-38026 Grenoble-Cedex, France,*
[10]*Université Bordeaux 1, IN2P3- CENBG - Le Haut-Vigneau BP120 33175, Gradignan Cedex, France*
(Dated: April 7, 2005)

High-spin states in the nucleus ^{102}Ru have been investigated via the ^{96}Zr(^{13}C,$\alpha 3n$) reaction at beam energies of 51 and 58 MeV, using the EUROBALL IV γ-ray spectrometer and the DIAMANT charged particle array. Several new high-spin bands have been established. The ground state band has been extended up to $E_x \sim 12$ MeV with $I^\pi = (26^+)$, while the previously published negative-parity bands have been extended up to $E_x \sim 11$ and ~ 9 MeV with $I^\pi = (23^-)$ and (20^-), respectively. The deduced high-spin structure has been compared with Woods-Saxon TRS calculations and, on the basis of the measured Routhians, aligned angular momenta, and $B(M1)/B(E2)$ ratios, $\nu h_{11/2}(g_{7/2}, d_{5/2})$ configurations are suggested for the negative-parity structures.

PACS numbers: 21.10.Hw,21.60.Ev,23.20.Lv,27.60.+j

I. INTRODUCTION

The structure of transitional nuclei near A$\sim$100 just below the tin isotope chain is characterized by valence hole-like protons in the $g_{9/2}$ orbital below the Z=50 gap and valence particle-like neutrons in the $d_{5/2}$, $g_{7/2}$, $h_{11/2}$ orbitals above the N=50 gap. In these configurations the protons occupy high-Ω orbitals, while the neutrons are situated in low-Ω ones. The different shape driving forces of the low- and high-Ω orbitals may lead to triaxial shapes due to the γ-softness of the core. Indeed, several nuclear structure phenomena related to triaxiality have been noted in this region. The occurrence of signature inversion has been reported in $^{98,100-103}$Rh [1] and recently chiral twin bands have been found in ^{104,105,106}Rh [2–4]. The observation of such structures provides experimental evidence for the existence of stable triaxial shapes. In a more recent work, excited states in ^{102}Ru have been studied by Lalkovski *et al.* [5] in the low-spin regime relevant for chiral symmetry breaking observed in the neighboring odd-odd nuclei. The nature of the triaxiality in ^{102}Ru (rigid or γ-soft) has been examined through an analysis of the excitation energies in the quasi-γ band.

Previously, the evolution from vibrational to rotational structure has been investigated by Regan *et al.* [6] by analyzing the positive parity yrast cascade of ^{102}Ru; a transition between these two modes has been clearly highlighted. In the incomplete fusion reaction ^{100}Mo(^{7}Li,$[p,d,t]xn\gamma)^{102}$Ru, two negative-parity bands have been identified in the lower-spin region by Dejbakhsh *et al.* [7]. The bottom part in one of them has been described as a sequence where octupole vibration may appear. The study of the negative-parity bands at higher spin can provide a further interesting insight into the change from vibrational to rotational motion.

An experiment with the primary goal of studying chirality in the rhodium isotopes near A$\sim$104 provided us with a significant amount of data on ^{102}Ru, thereby making it possible to extend its band structure. In section II we describe the experimental techniques, data evaluation, and results. The intepretation of the experimental findings is presented in section III.

II. EXPERIMENTAL METHODS AND RESULTS

The experiment was carried out at the Vivitron accelerator at IReS, Strasbourg. A ^{13}C beam impinged upon a stack of two targets, each of thickness 558 μg/cm^2 and enriched to 86% in ^{96}Zr. The emitted γ rays were

*On leave of absent from Faculty of Physics, St. Kliment Ohridski University of Sofia, BG-1164 Sofia, Bulgaria
†Deceased
‡Present address: Tohoku University, Department of Physics, Sendai 980-8578, Japan

detected by the EUROBALL IV detector array [8] which consisted of 15 cluster [9] and 26 clover [10] composite Ge detectors. The cluster detectors were placed at backward angles, while the clover detectors were positioned in two rings at an averaged angle of 90° relative to the beam direction. The γ rays were measured in coincidence with charged particles in order to eliminate the contaminants from the stronger (^{13}C,xn) reaction channels. The detection of light charged particles was performed by means of the highly efficient DIAMANT array which was composed of 88 CsI detector elements [11]. Protons and α-particles were discriminated by gating on a two dimensional spectrum containing the energy of the detected charged particles along one axis and their particle identification signal (PID) along the other axis. The PID is an electrically generated signal from the DIAMANT electronics [12] which uses a combination of ballistic deficit and zero cross-over timing.

A total of $\sim 2 \times 10^9$ triple- and higher-fold coincidence events were stored onto magnetic tapes among which $\sim 5 \times 10^8$ belonged to the ^{102}Ru reaction channel. The data obtained from the Ge detectors were sorted into a γγγ-coincidence cube by requiring the detection of an α-particle. For the analysis of the triple-coincidence cube a standard gating procedure was carried out with the help of the RADWARE software package [13]. Sample γ-ray gated spectra are shown in Fig. 1.

Energies and relative intensities of the γ-ray transitions of ^{102}Ru, determined from the γγγ-coincidence cube, are given in Table I. The Ge detectors were calibrated for both energy and efficiency using a ^{152}Eu source placed at the target position. The systematic errors due to the energy and efficiency calibrations were estimated to be ∼0.2-0.3 keV and ∼5%, respectively. A total of 72 transitions were assigned to ^{102}Ru, two thirds of which are observed the first time in the present work.

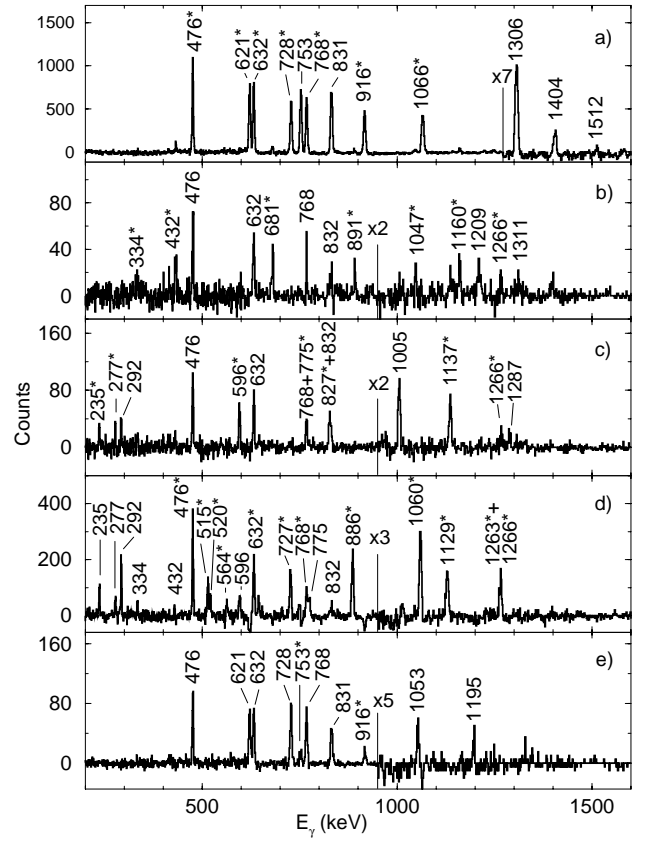FIG. 1: Sample background subtracted γγγ-coincidence spectra showing the observed bands in ^{102}Ru. The presented transitions are in simultaneous coincidence with the γ rays marked with asterisks and either the 1208 keV (a), the 1245 keV (b), the 1243 keV (c), the 988 keV (d), or the 1276 keV (e) transitions.

TABLE I: Energies, relative intensities, DCO ratios, linear polarisations, and deduced multipolarities of transitions assigned to ^{102}Ru in the present work.

E_γ(keV)	I_γ(rel.)	R_{DCO}	P	Mult.	E_i(keV)
196.6(5)	0.2(1)				3140
235.4(3)	4.6(3)	0.33(6)		D	2943
276.8(3)	2.6(2)	0.41(5)		D	2651
292.3(3)	7.2(4)	1.05(6)	0.51(18)	E2	2943
328.1(4)	0.3(1)	1.09(25)		Q	2374
333.6(5)	5.9(4)	0.99(6)	0.64(20)	E2	2708
386.3(4)	0.8(1)	0.98(11)	0.68(46)	M1+E2^a	3329
399.4(4)	1.6(2)	0.24(6)	-0.31(18)	M1+E2	3539
424.6(4)	1.3(2)	1.00(9)	0.89(54)	M1+E2^a	3860
432.0(3)	21.6(12)	1.09(5)	0.60(9)	E2	3140
475.7(3)	100.0(52)	1.01(5)	0.43(8)	E2	476
498.4(4)	0.4(1)				2374
514.6(4)	1.6(2)				3458
520.4(4)	0.7(1)	1.08(21)		Q	3458
545.4(4)	0.6(1)				4366
563.9(4)	1.2(2)	1.10(24)		Q	2938
595.9(3)	10.3(6)	0.98(5)	0.42(10)	E2	3539
621.2(3)	28.0(16)	0.99(5)	0.53(9)	E2	4056

TABLE I: continued

E_γ(keV)	I_γ(rel.)	R_{DCO}	P	Mult.	E_i(keV)
621.4(9)	0.3(1)				3329
632.2(3)	97.6(51)	1.00(5)	0.50(8)	E2	1108
645.6(5)	0.8(1)	0.53(9)	-0.42(18)	M1+E2	4185
664.6(4)	0.6(1)	1.10(19)	0.99(51)	M1+E2^a	4721
680.9(3)	13.9(8)	0.96(5)	0.35(10)	E2	3821
684.8(5)	0.8(1)	0.95(14)		Q	4014
727.1(4)	2.3(2)	0.99(8)		Q	4185
728.1(3)	35.6(20)	1.04(5)	0.56(9)	E2	3435
750.2(8)	0.4(1)				3458
752.8(3)	20.6(14)	1.03(5)	0.55(9)	E2	4809
767.7(3)	86.0(46)	1.00(5)	0.43(8)	E2	1876
775.4(3)	7.8(5)	1.07(6)	-0.75(22)	E1^a	2651
826.8(5)	0.5(1)				4841
827.2(3)	7.7(5)	1.01(6)	0.31(12)	E2	4366
831.4(3)	40.0(27)	1.00(5)	0.57(9)	E2	2707
831.9(3)	32.3(20)	0.55(5)	0.36(9)	E1	2708
860.8(5)	0.6(1)	1.03(5)		Q	4721
886.2(4)	1.9(2)	1.08(10)		Q	5071
891.3(3)	8.7(6)	0.92(5)	0.84(18)	E2	4712
916.3(3)	12.9(8)	0.94(6)	0.73(15)	E2	5725
919.6(5)	0.2(1)				7001

TABLE I: continued

E_γ(keV)	I_γ(rel.)	R_{DCO}	P	Mult.	E_i(keV)
926.8(7)	0.4(1)				5768
958.4(5)	0.9(1)	1.04(14)		Q	5679
958.8(5)	0.3(1)				6727
988.4(4)	1.3(2)	1.11(14)	0.95(32)	E2	6059
1005.3(3)	4.0(3)	0.95(7)	0.63(34)	E2	5371
1046.7(3)	4.9(3)	1.00(7)	0.53(17)	E2	5759
1053.0(4)	0.3(1)	1.08(19)		Q	8054
1060.0(4)	0.7(1)	0.94(10)		Q	7119
1061.9(9)	0.4(1)				2938
1065.8(3)	6.2(4)	0.99(6)	0.72(17)	E2	6791
1128.7(4)	0.4(1)	0.92(20)		Q	8248
1136.8(4)	2.1(2)	0.91(7)	0.86(36)	E2	6508
1152.7(4)	2.0(2)	0.96(11)	0.81(37)	E2	3860
1160.4(4)	2.0(2)	1.04(9)	0.76(32)	E2	6919
1195.1(4)	0.2(1)	0.94(12)		Q	9249
1207.9(4)	2.7(3)	0.99(6)	0.60(17)	E2	7999
1209.4(4)	0.5(1)	1.02(10)	1.15(57)	E2	8128
1243.2(4)	0.6(1)	1.10(20)		Q	7751
1244.6(4)	0.2(1)	1.07(14)		Q	9373
1250.3(5)	0.2(1)				9249
1262.7(6)	0.2(1)				9511
1263.2(4)	0.4(1)				8054
1266.2(4)	12.4(8)	0.50(6)	0.40(15)	E1	2374
1272.3(4)	0.6(1)				6081
1276.0(4)	0.9(2)	1.00(7)	1.02(48)	M1+E2[a]	7001
1286.1(4)	1.1(1)	1.02(17)		Q	4721
1286.9(8)	0.2(1)				9038
1306.2(4)	1.2(2)	1.01(9)	0.68(35)	E2	9305
1310.6(6)	0.1(1)				10684
1403.8(4)	0.3(1)	0.93(15)		Q	10709
1512.4(7)	0.1(1)				12221
1570.4(4)	0.4(1)	0.59(9)	1.05(87)	E1	2046
1622.7(5)	0.2(1)				5679

[a] indicates non-stretched ΔI=0 dipole transition.

In order to determine the multipolarities of the γ-ray transitions, an analysis of angular-correlation ratios based on the DCO formalism [14] was carried out. For the DCO analysis, data obtained from the cluster detectors mounted at an average angle of 156° and the clover detectors placed at about 90° were used. A non-symmetric $\gamma\gamma$-matrix, comprising of γ rays detected in the cluster detectors along one axis and in the clover detectors along the other axis, was created by requiring a coincidence with one α-particle. The ratios $R_{DCO}=I_{\gamma\gamma}(156°, 90°[\text{gate}])/I_{\gamma\gamma}(90°, 156°[\text{gate}])$ were extracted applying corrections for the different efficiencies of the clover and the cluster detector rings. Theoretical DCO ratios have been calculated for the experimental geometry as described in Ref. [3]. According to these estimates, a value of R_{DCO}=1.0 characterizes a stretched quadrupole transition and ≈0.6 a stretched dipole one, when gated by a stretched E2 γ ray. The expected R_{DCO} for a pure non-stretched dipole transition with δ≈0 multipole mixing ratio is approximately the same as for a stretched quadrupole transition. The attenuation coefficients of incomplete alignment were fitted to strong transitions with known multipolarities in the calculations. For mixed

M1+E2 transitions R_{DCO} ratios can vary between 0.5 and 1.0 depending on the δ mixing ratio of the γ ray [3]. The DCO ratios obtained in this way for previously known transitions in ^{102}Ru agree with existing assignments [6, 7]. The results of the DCO analysis are given in Table I.

The multipolarity assignments were further corroborated by extracting the electromagnetic character of the transitions by measuring the linear polarization of the γ rays. For this purpose, the four-element clover detectors placed close to 90° relative to the beam direction were used as Compton polarimeters [15]. Two matrices were constructed from $\gamma\gamma$-events detected in coincidence with one α-particle; single hits in any segment of the clover detectors were placed on one axis while the added-back double-hit scattering events were placed on the other axis. In the first matrix the scattering events took place perpendicular, while in the second matrix parallel to the reaction plane. The number of perpendicular ($N_\perp$) and parallel ($N_\parallel$) scatters for a given γ ray were obtained from spectra gated on the single-hit axis of the respective matrix by transitions in coincidence with the given γ ray. Assuming that each clover crystal has equal efficiency, an experimental linear polarization is defined as

$$P = \frac{1}{Q}\frac{N_\perp - N_\parallel}{N_\perp + N_\parallel}, \qquad (1)$$

where Q is the polarization sensitivity for the clover detectors, which is a function of the γ-ray energy [15]. $N_\perp$ and $N_\parallel$ denote the number of events scattered perpendicular and parallel to the reaction plane, respectively. P>0 is characteristic for stretched E1, E2 and non-stretched M1 transitions, while P<0 characterizes stretched M1 and non-stretched E1 transitions. The results of the linear polarisation analysis are summarized in Table I.

During the multipolarity assignments only dipole and electric quadrupole transitions were considered. In addition, it was assumed that in the heavy-ion induced fusion-evaporation reactions, high-spin states are preferably populated and their decays proceed mainly via stretched transitions along the yrast line. Thus, the maximum possible spin value allowed by the angular distribution ratios of the transitions was assigned to the states. Definite parity was proposed to a state if E1, M1 or quadrupole character could be determined for one of the transitions connecting it to a state with known parity. The multipolarities obtained are listed in Table I.

A. The level scheme of ^{102}Ru

A partial level scheme derived from the present experiment is shown in Fig. 2. It was constructed on the basis of triple-coincidence relations, as well as energy and intensity balances. The order of the γ rays in a cascade was determined by their relative intensities. Several new
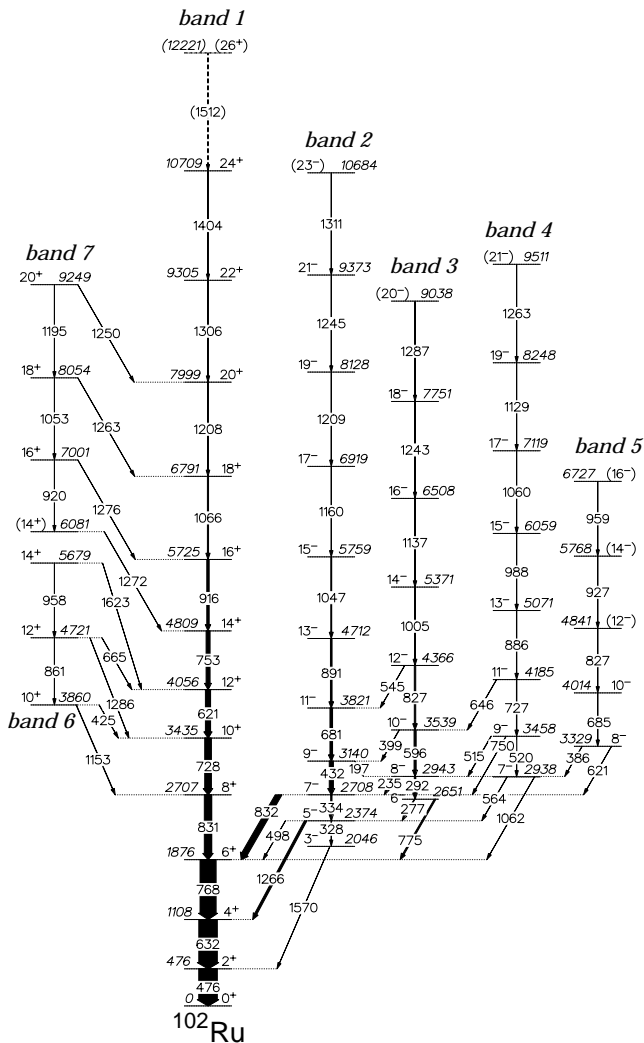
FIG. 2: The partial level scheme of ^{102}Ru obtained in the present work.

On the basis of the DCO and linear polarization analysis, stretched E2 and quadrupole character are assigned to the 1306 and the 1404 keV γ rays, respectively, suggesting I^π=22$^+$ and 24$^+$ values for the states at 9305 and 10709 keV. The 1512 keV γ ray is too weak to obtain information on its multipolarity. As this γ ray continues the rotational sequence, it is assumed to be a stretched E2 transition and a tentative I^π=(26$^+$) spin-parity value is assigned to the state at 12221 keV.

Band 2 has been previously reported up to I^π=(13$^-$) in Ref. [7]. In the present work it was confirmed and extended with five additional levels up to an excitation energy E_x=10.7 MeV. The corresponding γ-ray transitions are shown in Fig. 1 b) except for the gating 1245 keV γ ray. The multipolarities obtained for the transitions placed in the lower part of the band are in agreement with the previous spin-parity assignments [7]. The dipole nature and the linear polarization of the 832, 1266 and 1570 keV γ rays linking the band to the positive parity yrast sequence strengthen the negative parity assignment of *band 2*. Above the I^π=13$^-$ state, the stretched E2 or quadrupole character of the 1047, 1160, 1209, and 1245 keV transitions yield the spin-parity assignments of the 15$^-$, 17$^-$, 19$^-$ and 21$^-$ states. The intensity of the 1311 keV γ ray is not sufficient to draw a conclusion about its multipolarity, so the spin-parity assignment of the level at 10684 keV remains tentative.

The lower part of *band 3* up to I^π=10$^-$ has been identified in Ref. [7]. Our coincidence data support the previous placements of the 775, 277, 292, 235, and 596 keV transitions, and allow the extension of the band structure by five levels up to an excitation energy $E_x \approx$9 MeV, as shown in Fig. 1 c). The extracted multipolarities are in accordance with the former spin-parity assignments of *band 3* up to I^π=10$^-$. On the basis of the deduced stretched E2 or quadrupole characters of the 827, 1005, 1137 and 1243 keV γ rays, we propose 12$^-$, 14$^-$, 16$^-$ and 18$^-$ spin-parity values for the levels at 4366, 5371, 6508 and 7751 keV. The 1287 keV γ ray is too weak to determine its multipolarity. However, since this transition continues the rotational sequence, a tentative I^π=(20$^-$) spin-parity value is assigned to the state at 9038 keV.

Besides the previously reported structures, four new bands (*bands 4, 5, 6* and *7*) were found in the present experiment. The transitions placed in *band 4* are shown in Fig. 1 d) except for the gating 988 keV γ ray. On the basis of the coincidence relations this band is connected to the negative-parity *bands 2* and *3*, among others, by the quadrupole 564 keV and the M1+E2 646 keV γ rays, thereby firmly establishing negative parity for *band 4*. The stretched quadrupole nature of the 564 keV transition determines the I=7 spin assignment for the lowest level in the band at 2938 keV. Based on the extracted stretched E2 and quadrupole character of the 520, 727, 886, 988, 1060 and 1129 keV γ rays, I^π=9$^-$, 11$^-$, 13$^-$, 15$^-$, 17$^-$, and 19$^-$ spin-parities are deduced for the states up to E_x=8248 keV in *band 4*. Due to the insufficient intensity of the 1263 keV γ ray a tentative I^π=(21$^-$) value

bands (*bands 4, 5, 6, 7*) were found and connected to the previously reported ones (*bands 1, 2, 3*) which were themselves extended to higher excitation energy and spin. The placement of the known transitions is in agreement with the previous work [6, 7] except for some minor differences: (i) our coincidence data did not support the existence of the 843 keV γ ray assigned to ^{102}Ru by Dejbakhsh *et al.* [7]; (ii) on the basis of its coincidence relations the 827 keV transition in *band 3* is placed at a higher excitation energy than in Ref. [7], i.e. on the top of the 596 keV γ ray.

The yrast band (*band 1* in Fig. 2) has been previously observed up to 20 $\hbar$ [6]. Three further states were found in this band which decay by the 1306, the 1404 and the tentative 1512 keV transitions. In Fig. 1 a) the sum of triple γ-ray gate spectra shows clearly all the transitions placed in the yrast cascade. The deduced multipolarities are in agreement with the known spin-parity values for this band, thus we adopt these values up to I^π=20$^+$.

is assigned to the highest observed level in this band.

Band 5 is linked to the $I^\pi=8^-$ state in *band 3* via the 386 keV γ which has $R_{DCO}=0.98(11)$ and $P=0.68(46)$. According to these values, the 386 keV γ ray could in principle be a stretched E2 or a non-stretched M1+E2 transition. With the former possibility the levels in *band 5* would be yrast from the $I=10$ spin value. However, since *band 5* is rather weakly populated compared to the yrast ground state band, we adopt a $\Delta I=0$ M1+E2 multipolarity for the 386 keV transition and thus assign a spin-parity $I^\pi=8^-$ to the state at 3329 keV. This assignment is further corroborated by the existence of the 621 keV transition to the 7^- state of *band 2*. The spin-parity $I^\pi=10^-$ of the level at 4014 keV is suggested by the DCO ratio of the depopulating 685 keV γ ray. Although the γ rays placed higher in *band 5* are too weak to determine their multipolarities, as they continue the rotational cascade, they are assumed to be stretched E2 transitions. Thus, tentative (12^-), (14^-) and (16^-) spin-parity values are respectively assigned to the states at 4841, 5768 and 6727 keV.

The new γ-ray cascades of *bands 6* and *7* are connected to the ground state band by several transitions. In *band 6*, on the basis of the stretched quadrupole nature of the 1286 and the 958 keV γ rays, $I^\pi=12^+$ and 14^+ spin-parity values are proposed for the states at 4721 and 5679 keV excitation energies, respectively. As the level at 3860 keV is fed by the stretched quadrupole 861 keV transition, we propose an $I^\pi=10^+$ assignment to it. These spin-parity assignments are strengthened by the non-stretched M1+E2 multipolarities of the 425 and the 665 keV linking γ rays.

Some of the γ rays assigned to *band 7* are presented in Fig. 1 e). This band is linked to the ground state band among others by the 1276 keV transition. On the basis of its DCO ratio and linear polarization, a stretched E2 or a non-stretched M1+E2 multipolarity is possible for this γ ray. The stretched E2 assignment would suggest an $I^\pi=18^+$ spin-parity value for the level at 7001 keV. Since the 1053 and the 1195 keV γ rays, feeding this level in cascade, have stretched quadrupole characters, $I^\pi=20^+$ and 22^+ spin-parity values would be assigned to the states established at 8054 and 9249 keV. In this case *band 7* would become yrast which contradicts the fact that this band is populated about 6 times weaker than the yrast ground state band at this spin region. Thus, we accept the non-stretched M1+E2 multipolarity assignment to the 1276 keV γ ray, as well as, $I^\pi=16^+$, 18^+ and 20^+ spin-parity values for the states at 7001, 8054 and 9249 keV, respectively. The 920 and the 1272 keV γ rays do not have enough intensity to draw any conclusion on their multipolarities. As the 920 keV transition continues the rotational cascade down to a lower excitation energy, we assume a tentative (14^+) spin-parity value for the state at 6081 keV. No experimental evidence was found for the connection of *bands 6* and *7*.
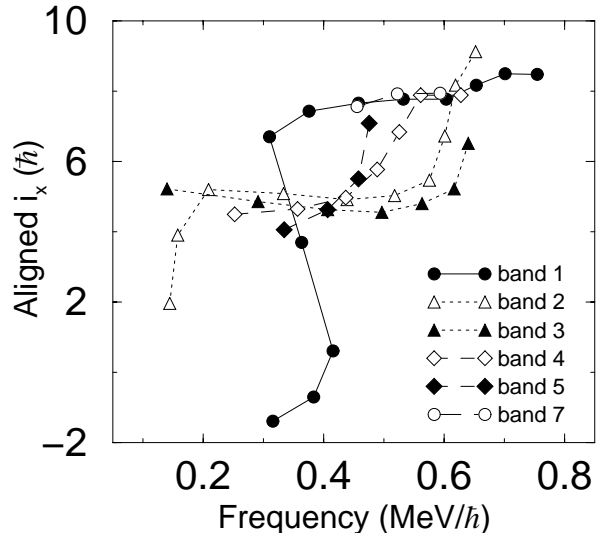

FIG. 3: Experimental alignments i_x of *bands 1-5* and *7*. A frequency-dependent moment-of-inertia reference was subtracted.

III.   DISCUSSION

In order to discuss the structure of the observed bands, their experimental Routhians (E') and aligned angular momenta (I_x,i_x) were extracted [16] and compared with total routhian surface (TRS) calculations based on the Woods-Saxon cranking formalism [17–19]. The i_x experimental alignments, which are plotted in Fig. 3, were obtained by subtracting a reference based on a variable moment of inertia $J_{ref}=J_0+\omega^2J_1$ with $J_0=14$ $\hbar^2\text{MeV}^{-1}$ and $J_1=15$ $\hbar^4\text{MeV}^{-3}$. The K quantum numbers assigned to the bands have been chosen to be 0 for the ground state band because it corresponds to the quasiparticle vacuum configuration at low rotational frequency. As it will be discussed in the followings, the negative parity bands are assigned as two-quasineutron configurations involving the [550]1/2 and one of the [411]3/2, [413]5/2 or [422]3/2 Nilsson orbitals, for which we assume to have K=1/2, 3/2, 5/2 and 3/2 values, respectively. Combining these values 1, 2 or 3 are the possible K values for these bands. We used an average value of 2 in calculating the alignments. We note that at higher spins the alignment in a band is not sensitive to varying the value of K by one or two units. For band 7 we also assumed K=2 because in the followings this band is assigned tentatively as β-vibration coupled to the ground-state band.

In ^{102}Ru at moderate deformations the neutron Fermi surface lies near the [411]3/2, [413]5/2 and [422]3/2 positive-parity Nilsson states originating from the $d_{5/2},g_{7/2}$ subshell, as well as the [550]1/2 and [541]3/2 negative-parity Nilsson states originating from the $h_{11/2}$ orbital. The proton Fermi surface lies in the middle of the unique parity $g_{9/2}$ subshell, close to the [303]5/2 and

TABLE II: Labels used for the quasineutron states for parity π and signature α with n denoting the nth such state.

$(\pi,\alpha)_n$	label	Shell model
$(+,+1/2)_1$	A	$d_{5/2}, g_{7/2}$
$(+,-1/2)_1$	B	$d_{5/2}, g_{7/2}$
$(+,+1/2)_2$	C	$d_{5/2}, g_{7/2}$
$(+,-1/2)_2$	D	$d_{5/2}, g_{7/2}$
$(-,-1/2)_1$	E	$h_{11/2}$
$(-,+1/2)_1$	F	$h_{11/2}$
$(-,-1/2)_2$	G	$h_{11/2}$
$(-,+1/2)_2$	H	$h_{11/2}$

[301]1/2 normal parity Nilsson orbitals. Among these Nilsson states, the high-j low-Ω [550]1/2 state is predicted to approach the Fermi surface most steeply with increasing rotational frequency. Thus the configurations of the lowest-energy excited rotational bands are expected to contain this orbital. The observed bands in ^{101}Ru [20] and ^{103}Ru [21] are in a good agreement with the above assumptions. In both nuclei the [550]1/2$^-$ band is yrast and the first alignment in the positive parity band corresponds also to the alignment of the [550]1/2 $h_{11/2}$ neutron pair. Moreover, in ^{101}Ru the [413]5/2$^+$ configuration is assigned to the observed positive-parity band.

Indeed, the positive-parity ground state band of ^{102}Ru (*band 1*) is known to have a predominantly $\nu(h_{11/2})^2$ configuration above the first crossing at $\hbar\omega \approx 0.4$ MeV [6, 7]. In accordance with this expectation, the alignment of a $h_{11/2}$ neutron pair is well established in Fig. 3 with nearly the full possible alignment gain of $\sim 10\hbar$. As the negative-parity bands do not show a similar alignment gain at ~ 0.4 MeV/$\hbar$, the $\nu h_{11/2}$ alignment seems to be blocked. This implies that their configuration includes one neutron in the $h_{11/2}$ orbit. The alignment plot suggests a two-quasiparticle configuration for these bands. According to the negative parity, the second quasineutron is expected to have a $g_{7/2}$, $d_{5/2}$ origin.

On the basis of these considerations, total routhian surface calculations were performed for the vacuum and two-quasineutron configurations which include one quasiparticle in the $h_{11/2}$ state and another one in the four lowest-energy positive-parity states. For labelling the lowest-energy quasineutron states the commonly used notations, given in Table II, are adopted.

A. The yrast positive-parity band 1

The experimental and TRS Routhians (E'), as well as the aligned angular momenta (I_x), are compared in Fig. 4 and 5, respectively. The theoretical E' curves are normalized so that the experimental and the TRS Routhians of the yrast band overlap each other. In the yrast sequence, the TRS calculations predict rotational structure only starting from spin values of 10-12 $\hbar$ after the alignment of a $h_{11/2}$ neutron pair. This prediction is in a good
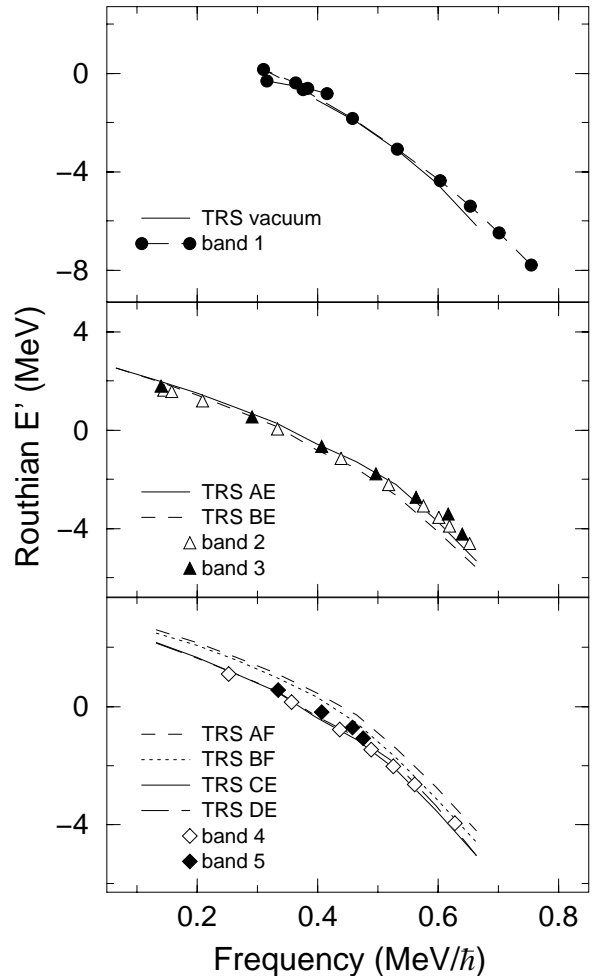

FIG. 4: Comparison of the experimental and TRS Routhians E' for *bands 1-5*.

agreement with the results of Ref. [6] where vibrational character is assigned to the low-spin part of the yrast band. Above spins of 10-12 $\hbar$ the TRS calculations give a good overall description of the Routhians and aligned angular momenta. One discrepancy is that although a definite alignment of two protons in the $g_{9/2}$ orbitals is predicted at ~ 0.55 MeV/$\hbar$ in the calculations, the experimental values show a more gradual change in I_x. The predicted shape starting from $\hbar\omega \approx 0.4$ MeV is characterized by $\beta_2 \approx 0.23$ and $\gamma \approx 16°$, while the $(g_{9/2})^2$ proton alignment drives it to slightly smaller $\beta_2 \approx 0.18$ and $\gamma \approx 10°$ values.

B. The negative-parity bands

To further investigate the possibility of the appearance of octupole vibration in the bottom part of *band 2* suggested in Ref. [7], we plotted the $R_{E-GOS} = E_\gamma(I \to I-2)/I$ versus I trajectories, so-called E-GOS curves (see Fig. 6), which are sensitive to a transition between vibra-
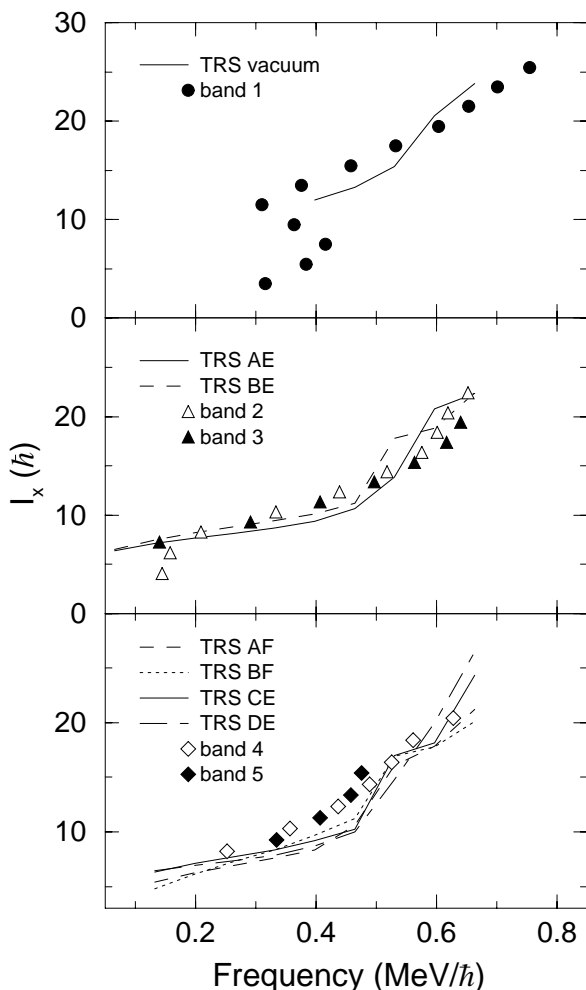
FIG. 5: Comparison of the experimental and TRS aligned angular momenta I_x for *bands 1-5*.

FIG. 6: E-GOS curves for *bands 1* and *2*.

the A or B $d_{5/2}, g_{7/2}$ orbitals. On the basis of the good agreement between the experimental and the TRS Routhians (see Fig. 4), we assign these predicted coupled bands with very small signature splitting having $\nu h_{11/2}(d_{5/2}, g_{7/2})$ configuration to *band 2* above spin $I \approx 9$ and to *band 3*.

In the case of *bands 2* and *3* the TRS aligned angular momentum curves (see Fig. 5) estimate the alignment of a $g_{9/2}$ quasiproton pair but at $\sim$50-70 keV/$\hbar$ lower frequency than the observed values; this might be due to a larger deformation than $\beta_2 \approx 0.15$ and $\gamma \approx 10°$ derived from the TRS calculations. It is worth mentioning that although the $\pi g_{9/2}$ alignment predicted by the TRS calculations is in a good agreement with the experimental results except for the more gradual increase in the experimental curves, at $\sim$0.5 MeV/$\hbar$ frequency other quasineutron alignments can appear, as well. In nuclei with A$\sim$100 below the Z=50 shell closure the $\pi g_{9/2}$, the $\nu g_{7/2}$ and the second $\nu h_{11/2}$ alignments can be situated nearby in frequency as discussed in Ref. [22]. On the basis of the available experimental data the possibility of the rotational alignment of the first pair of $\nu g_{7/2}$ or the second pair of $\nu h_{11/2}$ quasineutrons can not be excluded. However, according to Ref. [23] the $\pi g_{9/2}$ alignment is more probable in Ru isotopes because with decreasing proton number in this region the $\nu(g_{7/2})^2$ crossing is pushed up to higher frequencies.

It was also predicted by Dejbakhsh *et al.* [7] that in the even-even Ru isotopes with A$\approx$100 above I=8 the octupole becomes a dominant deformation mode and an 8^+, 9^-, 10^+ .... alternating positive, negative parity band corresponding to a rotating octupole shape could appear. On the contrary, such a structure was observed neither in the neighbouring ^{100}Ru nor in ^{102}Ru nuclei. In the study of the band structures in ^{100}Ru [24], several negative-parity bands were found and $\nu h_{11/2}(d_{5/2}, g_{7/2})$ two-quasineutron configurations were assigned to them, similarly to ^{102}Ru in the present work.

tional and rotational states [6]. The sharp, hyperbolic decrease in R_{E-GOS} provides a clear signature of a vibrational regime, while for a rotational structure R_{E-GOS} slightly increases at first at low spins and it then remains asymptotically flat. The vibration-to-rotation change for the positive parity yrast band of ^{102}Ru has been clearly demonstrated by Ref. [6]. In Fig. 6 we compare the E-GOS curves for *bands 1* and *2*. The behaviour of the E-GOS curve of *bands 2* is in a good agreement with the assumption that at low spins *bands 2* corresponds to a vibration structure [7], while for higher spins it has a rotational character.

On the basis of these findings *band 2* above spin $I \approx 9$ and *band 3* are discussed applying the rotational approach. As it is shown by their experimental alignments i_x in Fig. 3 and pointed out earlier, the higher spin part of *band 2* and *band 3* have similar two-quasineutron characters. The lowest energy negative-parity two-quasineutron configurations are expected to involve one quasineutron from the E $h_{11/2}$ orbital and another quasineutron from
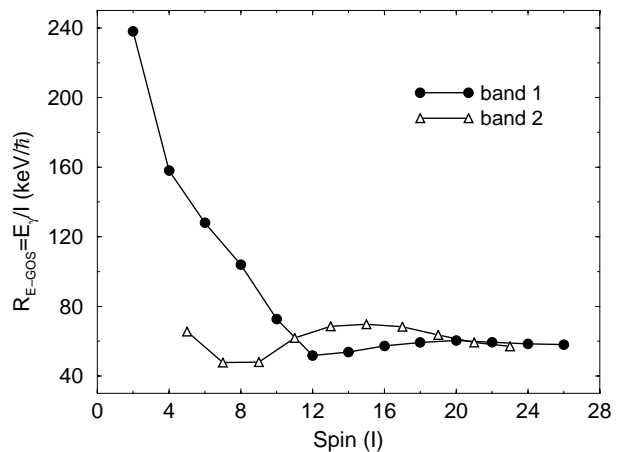
Bands 4 and *5* show alignment behaviour similar to *bands 2* and *3* as can be seen in Fig. 3. According to the TRS calculations, one quasineutron placed in the E $h_{11/2}$ orbital and the other one in the C or D $d_{5/2}, g_{7/2}$ orbitals can account for the next lowest energy negative-parity configurations. Based on the good agreement between the experimental and the TRS Routhians (see Fig. 4) we propose a $\nu h_{11/2}(d_{5/2}, g_{7/2})$ configuration for *bands 4* and *5*. For the CE and DE states the calculations predict decreasing deformation ($\beta_2 \approx 0.21$ to 0.15) and triaxiality ($\gamma \approx 23°$ to $10°$) values similarly to the AE and BE $\nu h_{11/2}(d_{5/2}, g_{7/2})$ states.

C. Analysis of the $B(M1)/B(E2)$ ratios

In order to strengthen the assignment of the quasiparticle configurations of the observed negative-parity bands, experimental $B(M1; I \rightarrow I-1)/B(E2; I \rightarrow I-2)$ ratios of reduced transition probabilities have been extracted from the measured $I_\gamma(M1)/I_\gamma(E2)$ branching ratios for *band 3*. The $B(M1)/B(E2)$ ratios within a coupled band are sensitive to the quasiparticle configuration of the band. For *bands 2, 4* and *5* the ratios could not be obtained as there are no observed M1 transitions to the corresponding coupled partner band. The $B(M1)/B(E2)$ ratios for *band 3* were extracted using the expression

$$\frac{B(M1; I \rightarrow I-1)}{B(E2; I \rightarrow I-2)} = \qquad (2)$$
$$= 0.697 \frac{E_\gamma^5(E2)}{E_\gamma^3(M1)} \frac{I_\gamma(M1)}{I_\gamma(E2)} \frac{1}{1+\delta^2} \left(\frac{\mu_N}{eb} \right)^2,$$

where the energies of the γ rays are given in MeV. The branching ratios were determined by setting gates on the transitions above the decaying level. The δ-multipole mixing ratios of the $\Delta I=1$ transitions were assumed to be small, and thus δ^2 can be neglected. The experimental $B(M1)/B(E2)$ ratios were compared to calculated values obtained using the following generalized expression formulated in Refs. [25, 26] and based on the geometrical model of Dönau and Frauendorf [27],

$$\frac{B(M1; I \rightarrow I-1)}{B(E2; I \rightarrow I-2)} = \frac{12}{5Q_0^2 \cos^2(\gamma+30)} \times \qquad (3)$$
$$\left[1 - K^2 \left(I - \frac{1}{2} \right)^{-2} \right]^{-2} \left\{ \left(1 - \frac{K^2}{I^2} \right)^{1/2} \times \right.$$
$$\left[K_1(g_1 - g_R) \left(1 \pm \frac{\Delta e'}{\hbar \omega} \right) + \sum_n K_n(g_n - g_R) \right] -$$
$$\left. \frac{K}{I} \left[(g_1 - g_R)i_1 + \sum_n (g_n - g_R)i_n \right] \right\}^2 .$$

Here K_n, g_n and i_n denote the K-value, g-factor and aligned angular momentum of the quasiparticles involved in the studied configuration, while g_R and

TABLE III: Parameters used to calculate $B(M1)/B(E2)$ ratios.

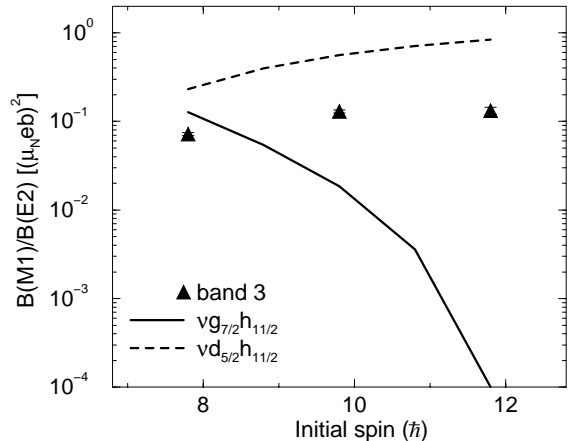| Configuration	g-factor	K-value	i_x
$\nu d_{5/2}$	-0.26	1.5	1.5
$\nu g_{7/2}$	+0.3	1.5	1.5
$\nu h_{11/2}$	-0.19	0.5	4.5

FIG. 7: Experimental and calculated $B(M1)/B(E2)$ ratios of *band 3*.

$K = K_1 + \sum_n K_n$ denote the rotational g-factor and the total K-value of the configuration, respectively. K_1, g_1 and i_1 refer to particles causing the signature splitting ($\Delta e'$), which was taken to be 0 in these calculations. In the present calculations K_n and i_n were approximated with constant values, and are listed in Table III together with the appropriate g_n values taken from [28]. The rotational gyromagnetic factor was taken as $g_R = Z/A$, while the Q_0 electric quadrupole moments and the γ-shape parameters were derived from the nuclear shape predicted by the TRS calculations.

The experimental and the calculated $B(M1)/B(E2)$ ratios for *band 3* are plotted in Fig. 7. The observed $B(M1)/B(E2)$ ratios fall between the theoretical curves obtained for $\nu g_{7/2} h_{11/2}$ and $\nu d_{5/2} h_{11/2}$ configurations, which further corroborates the suggested configuration for the negative parity *bands 2* and *3*.

D. The positive-parity bands 6 and 7

The lowest energy positive-parity quasiparticle excitations relative to the yrast band are expected to involve two additional quasineutrons from the A, B, C or D $d_{5/2}, g_{7/2}$ orbitals. However, the TRS calculations predict these configurations ~ 2 MeV higher in energy and ~ 10-$12\,\hbar$ higher in alignment than the corresponding values of *band 6*. Otherwise, this band decays to *band 1* by several transitions along the entire observed γ cascade which does not support the scenario of two-quasiparticle excitation, it rather indicates vibration coupled to the

yrast band. In addition, the energy difference between the 8^+ state in *band 1* and the lowest-lying observed state in *band 6* with $I^\pi = 10^+$ is ~ 1.1 MeV similar to the value between the 0^+ ground state and the 2^+ state in the γ-vibrational band linked to the low-spin region of the yrast band reported in Ref. [5]. These indicate that *band 6* might be a γ-vibrational band coupled to the $\nu(h_{11/2})^2$ configuration.

In the case of *band 7* although the experimental Routhians fall reasonably close to the TRS curves belonging to the AB and CB two-quasineutron configurations, and the calculations estimate the trend of the aligned angular momenta well, the theoretical values are predicted 4-5 $\hbar$ higher than the corresponding experimental ones. Furthermore, *band 7* follows the alignment values of the yrast band very well at around 0.5 MeV/$\hbar$ frequency, as can be seen from Fig. 3. *Band 7* is also connected to *band 1* by intense transitions along the observed γ-ray sequence like *band 6*. On the basis of these observations, *band 7* is assumed to have the same two-quasineutron configuration as *band 1* has in this spin region. γ- or β-vibrational bands are expected to show the above features. The facts that the odd-spin partner band to *band 7* was not observed and no links to *band 6* were found, favour the scenario of *band 7* being the β-vibrational band associated with the yrast cascade.

IV. SUMMARY

High-spin states of ^{102}Ru have been studied via the ^{96}Zr(^{13}C,$\alpha 3n$) reaction using the EUROBALL IV γ-ray spectrometer equipped with the DIAMANT array for the detection of charged particles. All previously known bands have been extended to higher spins and additional bands found. Comparing the experimental Routhians and aligned angular momenta to the predictions of Woods-Saxon TRS calculations, $\nu h_{11/2}(d_{5/2}, g_{7/2})$ configurations have been assigned to the observed negative-parity bands. On the basis of their connections to the yrast band and aligned angular momenta, the higher-lying positive-parity bands might have vibrational character.

[1] S. Chattopadhyay *et al.*, Phys. Rev. **C 57**, R471 (1998); J. Timár *et al.*, Nucl. Phys. **A 696**, 241 (2001); J. Gizon *et al.*, Nucl. Phys. **A 658**, 97 (1999); J. Timár *et al.*, Acta Phys. Pol. B **33**, 493 (2002); R.-R. Zheng *et al.*, Chin. Phys. Lett. **21**, 1475 (2004).

[2] C. Vaman *et al.*, Phys. Rev. Lett. **92**, 032501 (2004).

[3] J. Timár *et al.*, Phys. Lett. **B598**, 178 (2004).

[4] P. Joshi *et al.*, Phys. Lett. **B595**, 135 (2004).

[5] S. Lalkovski *et al.*, Phys. Rev. **C 71**, 034318 (2005).

[6] P.H. Regan *et al.*, Phys. Rev. Lett. **90**, 152502 (2003).

[7] H. Dejbakhsh and S. Bouttchenko, Phys. Rev. **C 52**, 1810 (1995).

[8] J. Simpson, Z. Phys. **A358**, 139 (1997).

[9] J. Eberth *et al.*, Nucl. Instr. Meth. **A369**, 135 (1996).

[10] G. Duchêne *et al.*, Nucl. Instr. Meth. **A432**, 90 (1999).

[11] J.N. Scheurer *et al.*, Nucl. Instr. and Meth. **A 385**, 501 (1997).

[12] J. Gál *et al.*, Nucl. Instr. and Meth. **A 516**, 502 (2004).

[13] D.C. Radford, Nucl. Instr. Meth. **A 361**, 297 (1995).

[14] A. Krämer-Flecken *et al.*, Nucl. Instrum. Methods **A 275**, 333 (1989).

[15] P.M. Jones *et al.*, Nucl. Instrum. Methods **A 362**, 556 (1995).

[16] R. Bengtsson and S. Frauendorf, Nucl. Phys. **A 327**, 139 (1979).

[17] W. Nazarewicz *et al.*, Nucl. Phys. **A 467**, 437 (1987).

[18] W. Nazarewicz *et al.*, Nucl. Phys. **A 503**, 285 (1989).

[19] R. Wyss *et al.*, Phys. Lett. **215B** 211, (1988).

[20] A.D. Yamamoto *et al.*, Phys. Rev. **C 66**, 024302 (2002).

[21] N. Fotiades *et al.*, Phys. Rev. **C 58**, 1997 (1998).

[22] P.H. Regan *et al.*, J. Phys. G **19**, L157 (1993).

[23] P.H. Regan *et al.*, Phys. Rev. **C 68**, 044313 (2003).

[24] J. Timár *et al.*, Phys. Rev. **C 62**, 044317 (2000).

[25] D.C. Radford *et al.*, Nucl. Phys. **A 545**, 665 (1992).

[26] S. Törmänen *et al.*, Nucl. Phys. **A 572**, 417 (1993).

[27] F. Dönau and S. Frauendorf, Proc. Conf. on High Angular Momentum Properties of Nuclei (Oak Ridge, Ed. N.R. Johnson, New York, Harwood Academic), (1983) p. 143; F. Dönau, Nucl. Phys. **A 471**, 469 (1987).

[28] A.M. Bizetti-Sona *et al.*, Z. Phys. **A 335**, 365 (1990); P. Raghavan, At. Data Nucl. Data Tables **42**, 189 (1989).